Lattice study on η_{c2} and $X(3872)$

Yi-Bo Yang,[1] Ying Chen,[1,2,*] Long-Cheng Gui,[1,2] Chuan Liu,[3] Yu-Bin Liu,[4] Zhaofeng Liu,[1,2]
Jian-Ping Ma,[5] and Jian-Bo Zhang[6]

(CLQCD Collaboration)

[1]*Institute of High Energy Physics, Chinese Academy of Sciences, Beijing 100049, China*
[2]*Theoretical Center for Science Facilities, Chinese Academy of Sciences, Beijing 100049, China*
[3]*School of Physics and Center for High Energy Physics, Peking University, Beijing 100871, China*
[4]*School of Physics, Nankai University, Tianjin 300071, China*
[5]*Institute of Theoretical Physics, Chinese Academy of Sciences, Beijing 100080, China*
[6]*Department of Physics, Zhejiang University, Zhejiang 310027, China*

Properties of 2^{-+} charmonium η_{c2} are investigated in quenched lattice QCD. The mass of η_{c2} is determined to be 3.80(3) GeV, which is close to the mass of D-wave charmonium $\psi(3770)$ and in agreement with quark model predictions. The transition width of $\eta_{c2} \to \gamma J/\psi$ is also obtained with a value of $\Gamma = 3.8(9)$ keV. Since the possible 2^{-+} assignment to $X(3872)$ has not been ruled out by experiments, our results help to clarify the nature of $X(3872)$.

I. INTRODUCTION

Even though the charmoniumlike resonance $X(3872)$ has been established for several years [1–4] with $M_X = 3871.68 \pm 0.17$ MeV and $\Gamma_X < 1.2$ MeV [5,6], the very nature of it has not been fully understood till now. Its even C parity has been firmly established from its decay to $J/\psi\rho$ [7] and to $J/\psi\gamma$ [8]. Further analysis of its decay angular distribution also constrains its total quantum number J^{PC} to be either 1^{++} or 2^{-+}. The discovery of $X(3872)$ has triggered quite a number of theoretical interpretations by assuming a quantum number 1^{++}, such as the radial excitation of χ_{c1}, the $D\bar{D}^*$ molecule [9–11], a tetraquark state [12–14], etc.; however, none of them can accommodate all the observed features of $X(3872)$. The situation became more complicated when the *BABAR* Collaboration reported in 2009 that 2^{-+} is more favored by the study of the decay angular distribution of the process $X(3872) \to J/\psi\pi^+\pi^-\pi^0$ [15]. In contrast, the same analysis by the Belle Collaboration claims that both the 1^{++} and 2^{-+} assignments are consistent with their data [6,16]. Another controversial result comes from the measurements of the radiative decays of $X(3872)$. For the decay mode $X(3872) \to \gamma J/\psi$, the *BABAR* and Belle collaborations reported consistent measurements [17,18]:

$$\mathrm{Br}(B^\pm \to X(3872)K^\pm)\mathrm{Br}(X(3872) \to J/\psi\gamma)$$
$$= (2.8 \pm 0.8 \pm 0.1) \times 10^{-6} \ (BABAR),$$
$$\mathrm{Br}(B^\pm \to X(3872)K^\pm)\mathrm{Br}(X(3872) \to J/\psi\gamma)$$
$$= (1.78^{+0.48}_{-0.44} \pm 0.12) \times 10^{-6} \ (Belle). \qquad (1)$$

With the world average value $\mathrm{Br}(B^+ \to X(3872)K^+) < 3.2 \times 10^{-4}$, one can estimate the branch ratio $\mathrm{Br}(X(3872) \to J/\psi\gamma) > 0.9\%$ (*BABAR*) or 0.6% (Belle). However, for the decay mode $X(3872) \to \gamma\psi'$, *BABAR* measured a 3.4 ± 1.4 times larger branch ratio [17], but Belle found no evidence [18]. This large discrepancy should be reconciled by further experimental measurements.

Theoretically, if we are constrained to its charmonium assignments, $X(3872)$ can be either the radial excitation of χ_{c1} (if 1^{++}), say, χ'_{c1}, or the $^1D_2$ charmonium η_{c2} (if 2^{-+}). The potential quark model predicts the mass of χ'_{c1} to be 3925 MeV [19], which deviates from the mass of $X(3872)$ by about 50 MeV. There are also many lattice studies predicting a χ'_{c1} mass ranging from 3850 to 4060 MeV [20–23], but with various uncertainties of their own, where the key difficulty is the challenging task of extracting the excited states. As for the η_{c2}, the quark models usually predict the mass to be in the range 3770 to 3830 MeV [19,24,25], which is even further away from the mass of $X(3872)$. This is also reinforced by recent lattice studies (and this work). At any rate, the mass parameter should not be the unique criterion for the interpretation of $X(3872)$; more information is definitely desired—for example, the radiative transition properties of χ'_{c1} and η_{c2}, which are theoretically accessible and hopefully can shed some light on the nature of $X(3872)$.

In this work, we will focus on the study of the properties of η_{c2}, such as its mass and radiative transition width to J/ψ. There are actually several phenomenological studies on this topic [26–28], but they are rather model dependent. In contrast, the lattice QCD approach, as a method from first principles, can provide information that is more model independent. An additional technical advantage in the

*cheny@ihep.ac.cn

study of η_{c2} on the lattice is that it is the ground state in the 2^{-+} channel and is free from the uncertainty of the extraction of excited states. In view of the notorious bad signal-to-noise ratio for P and D wave states, we adopt the quenched approximation so as to obtain large enough statistics for precise physical quantities to be derived. As for the quenched approximation, even though long-term experiences show that it is safe for charm quark systems, and the resultant uncertainties can be small, we still take several steps to check this and be assured of our results. We first calculate the spectrum of the ground state charmonia, such as $1S$, $1P$ states, and make sure that the experimental spectrum patterns are reproduced. As for the radiative transitions, we choose the transition mode of the tensor charmonium χ_{c2} to J/ψ as a calibration of the systematic uncertainties of our formalism by comparing our result to the experimental value. After that, we continue to the study of the radiative transition of η_{c2} to J/ψ. All the lattice calculations are carried out on anisotropic lattices which are suitable to the study of heavy particles. The numerical techniques are standard: the mass spectra are extracted from two-point functions, and the multipole amplitudes contributing to the transition widths are derived from the calculation of relevant three-point functions with a local electromagnetic current insertion. We apply two anisotropic lattices with different lattice spacings to estimate the lattice artifacts owing to the finite lattice spacing.

This work is organized as follows: The formalism for the calculation of radiative transition widths on the lattice is briefly introduced in Sec. II. In Sec. III are the numerical details, where the lattice setup, the extraction of mass spectra and transition form factors are explained, and the numerical results are presented. Section IV is the conclusion and discussion. The theoretical derivation of the multipole form factors is described in the Appendixes.

II. FORMALISM

As mentioned above, in this work we aim at the lattice calculation of the radiative transition rate of η_{c2} to J/ψ. The general radiative transition width of an initial particle i to a final particle f is

$$\Gamma(i \to \gamma f) = \int d\Omega_q \frac{1}{32\pi^2} \frac{|\vec{q}|}{M_i^2} \frac{1}{2J_i + 1} \sum_{r_i, r_f, r_\gamma} |M_{r_i, r_f, r_\gamma}|^2, \quad (2)$$

where $\vec{q} = \vec{p}_i - \vec{p}_f$ is the decay momentum with the mass-on-shell value $|q| = (M_i^2 - M_f^2)/(2M_i)$, M_i and M_f are the masses of the particles i and f, and M_{r_i, r_f, r_γ} is the transition amplitude with r_i, r_f, r_γ being the polarizations of i, f, and the photon, respectively. To the lowest order of QED, the amplitude M is expressed explicitly as

$$M_{r_i, r_f, r_\gamma} = \epsilon_\mu^*(\vec{q}, r_\gamma) \langle f(\vec{p}_f, r_f) | j_{\text{em}}^\mu(0) | i(\vec{p}_i, r_i) \rangle, \quad (3)$$

where $\epsilon_\mu^*(\vec{q}, r_\gamma)$ is the polarization vector of the photon, and $\langle f(\vec{p}', r_f) | j_{\text{em}}^\mu(0) | i(\vec{p}, r_i) \rangle$ gives the on-shell matrix

elements of the electromagnetic current $j_{\text{em}}^\mu(x) = \bar{\psi} Q \gamma^\mu \psi(x)$ between the i and f states. [Here ψ refers to an array of all the contributing quark flavors, such as $u, d, s, c, \ldots$, and Q is a diagonal matrix of quark electric charges, say, $\text{diag}(Q) = Q_u, Q_d, Q_s, Q_c, \ldots$.] The hadronic matrix element can be derived directly from the lattice QCD calculation of the related three-point functions:

$$\Gamma_{mn}^{(3)\mu}(\vec{p}_f, \vec{q}, t, t') = \sum_{\vec{x}, \vec{y}} e^{-i\vec{p}_f \cdot \vec{x}} e^{+i\vec{q} \cdot \vec{y}}$$
$$\times \langle O_m^f(\vec{x}, t) j_{\text{em}}^\mu(\vec{y}, t') O_n^{i\dagger}(\vec{0}, 0) \rangle, \quad (4)$$

where $O_{m,n}^{i,f}$ are the interpolating fields for the particles i and f, with the indices m, n referring to different spatial components for spin nonzero states. The explicit derivation can be expressed as

$$\Gamma_{mn}^{(3),\mu}(\vec{p}_f, \vec{q}, t, t') = \sum_{r_i, r_f} e^{-E_f t} e^{-(E_i - E_f) t'}$$
$$\times \frac{\hat{Z}_m^f(\vec{p}_f, r_f) \hat{Z}_n^{i*}(\vec{p}_i, r_i)}{2E_i 2E_f} \langle f(\vec{p}_f, r_f)$$
$$\times | j_{\text{em}}^\mu(0) | i(\vec{p}_i, r_i) \rangle (t', t - t' \to \infty), \quad (5)$$

where $\hat{Z}_m^{i,f}$ are the matrix elements like $\hat{Z}_m^X(\vec{p}_X, r_X) = \langle 0 | O_m^X | X(\vec{p}_X, r_X) \rangle$, which can be derived from the relevant two-point functions,

$$\Gamma_{X,mn}^{(2)}(\vec{p}_X, t) = \sum_{\vec{x}} e^{i\vec{p}_X \cdot \vec{x}} \langle O_m^X(\vec{x}, t) O_n^{X\dagger}(\vec{0}, 0) \rangle$$
$$\to \frac{1}{2E_X} e^{-E_X t} \sum_{r_X} \langle 0 | O_m^X | X(\vec{p}_X, r_X) \rangle$$
$$\times \langle X(\vec{p}_X, r_X) | O_n^{X\dagger} | 0 \rangle \quad (t \to \infty). \quad (6)$$

On the other hand, in the Minkowski space-time, the matrix elements $\langle f(\vec{p}_f, r_f) | j_{\text{em}}^\mu(0) | i(\vec{p}_i, r_i) \rangle$ can be generally expressed by several Lorentz-invariant form factors $F_k(Q^2)$ and Lorentz-covariant kinematic factors $\alpha_k(p_i, p_f)$ through the multipole decomposition,

$$\langle f(\vec{p}_f, r_f) | j_{\text{em}}^\mu(0) | i(\vec{p}_i, r_i) \rangle = \sum_k \alpha_k^\mu(p_i, p_f) F_k(Q^2), \quad (7)$$

where $p_{i,f}$ are now the four-momenta of particles i and f, and Q^2 is the squared transfer momentum $Q^2 = -(p_i - p_f)^2$. Obviously, the concrete form factors $F_k(Q^2)$ and the explicit expressions of the kinematic factors α_k depend on the properties of the particles i and f, and therefore should be worked out case by case. Finally, the decay width with an on-shell photon ($Q^2 = 0$) can be expressed as

$$\Gamma(i \to \gamma f) \propto \sum_k F_k^2(0). \quad (8)$$

So the key problem in this work is to reliably extract these form factors through the lattice calculation of the relevant

hadronic two-point functions and three-point functions described above.

III. NUMERICAL DETAILS

We use the quenched approximation in this study. The gauge configurations are generated by the tadpole improved gauge action [29] on anisotropic lattices with the temporal lattice much finer than the spatial lattice, say, $\xi = a_s/a_t \gg 1$, where a_s and a_t are the spatial and temporal lattice spacings, respectively. The much finer lattice in the temporal direction yields a higher resolution to hadron correlation functions, such that the masses of heavy particles can be tackled on relatively coarse lattices. We have two anisotropic lattices ($L^3 \times T = 8^3 \times 96$ and $12^3 \times 144$) with $\xi = 5$. The relevant input parameters are listed in Table I, where the lattice spacings, say, $a_s = 0.222(2)$ fm for the coarser lattice and $a_s = 0.138(1)$ fm for the finer lattice, are determined from $r_0^{-1} = 410(20)$ MeV by calculating the static potential. For each lattice, we generate 1000 configurations, each of which is separated by 500 heat-bath updating sweeps to avoid the autocorrelation. For fermions, we use the tadpole improved clover action for anisotropic lattices [30]. The parameters in the action are tuned carefully by requiring that the physical dispersion relations of vector and pseudoscalar mesons are correctly reproduced at each bare quark mass [31]. The bare charm quark masses for the two lattices are set by the physical mass of J/ψ $m_{J/\psi} = 3.097$ GeV.

In this work, we only consider the connected diagrams in the calculation of two-point and three-point functions. The contribution of the disconnected diagrams is assumed to be small for charmonium states due to the OZI suppression.

A. Ground-state charmonium spectrum

As the first step, we carry out a careful study on the ground-state charmonium spectrum, which can illustrate to some extent the systematic uncertainties due to the quenched approximation. For the states $\eta_c(0^{-+})$, $J/\psi(1^{--})$, $h_c(1^{+-})$, $\chi_{c0}(0^{++})$, and $\chi_{c1}(1^{++})$, we adopt the conventional quark bilinear operators like $\bar{c}\Gamma c$, with $\Gamma = \gamma_5$, γ_i, σ_{ij}, 1, and $\gamma_5\gamma_i$, respectively. For the tensor mesons $\chi_{c2}(2^{++})$ and $\eta_{c2}(2^{-+})$, since there are not quark bilinear operators, we build the corresponding operators by combining the quark bilinear operator with either the spatial gauge-covariant derivatives D_i or the color magnetic field strength operator B_i, which is built from Wilson

TABLE I. Relevant input parameters for this work. The spatial lattice spacing a_s is determined from $r_0^{-1} = 410(20)$ MeV by calculating the static potential.

β	ξ	a_s (fm)	La_s (fm)	$L^3 \times T$	N_{conf}
2.4	5	0.222	1.78	$8^3 \times 96$	1000
2.8	5	0.138	1.66	$12^3 \times 144$	1000

loops. It is known that the spin $J = 2$ states in the continuum correspond to both the T_2 and E irreducible representations (irreps) of the cubic point group O on finite lattices, so the interpolating field operators of the two irreps are constructed for the tensor charmonia. For example, the T_2 operator for the $\chi_{c2}(2^{++})$ state is taken as $|\epsilon_{ijk}|\bar{c}\gamma_j\overleftrightarrow{D}_k c$ where $\overleftrightarrow{D} = \overleftarrow{D} - \overrightarrow{D}$, and the E operator is also built to check the restoration of the continuum rotation symmetry.

We will emphasize the choice of the operators for the 2^{-+} state, which is the major object of this work. The situation for the η_{c2} meson is a little bit more complicated. We try first three types of operators, such as

$$|\epsilon_{ijk}|\bar{c}(x)\Sigma_j\overleftrightarrow{D}_k c(x) \quad (D\text{-type}),$$

$$|\epsilon_{ijk}|\bar{c}(x)\gamma_5\overleftrightarrow{D}_j\overleftrightarrow{D}_k c(x) \quad (DD\text{-type}),$$

$$|\epsilon_{ijk}|\bar{c}(x)\gamma_j B_k c(x) \quad (F\text{-type}),$$

where only the T_2 operators are presented (E operators can be built similarly, and the details can be found in Ref. [32]).

It is known that the signal-to-noise ratios of the correlation functions are always bad for P-wave and D-wave states. To circumvent this difficulty, we adopt the Coulomb-gauge fixed wall source techniques in the calculation of the spectrum. The configurations are fixed to the Coulomb gauge first, then the charm quark propagators are calculated with uniform wall source vectors. For the spin $J = 0$, 1 states, the point-sink wall source correlation functions can be constructed straightforwardly with these propagators. For the tensors, we use the F-type operators as the wall source, which means that additional inversions should be carried out with wall sources multiplied by the local color field strength operators $B_i(x)$. On the other hand, since the gauge is fixed, the gauge-covariant derivative operator $\overleftrightarrow{D}$ is replaced by the direct derivative operator $\overleftrightarrow{\nabla} = \overleftarrow{\nabla} - \overrightarrow{\nabla}$ in the practical calculation.

The masses of $1S$ and $1P$ charmonium states can be neatly derived with the standard data analysis; however, the situation for the 2^{-+} channel is very strange. Figure 1 shows the effective masses of various correlation functions of this channel at $\beta = 2.8$. It is seen that the effective mass of the F-type point sink and F-type wall source correlator (F-F) saturates at a plateau with the best-fit mass 4.43 (8) GeV, while that of the DD-type point sink and F-type wall source correlator (DD-F) goes lower and does not show a perfect plateau. Intuitively, a mass of 4.4 GeV is too large for the 2^{-+} ground-state charmonium. Thus, what one can infer from these behaviors is that the F-type operator couples predominantly to a higher state but little to the conventional charmonium; in the mean time, there must be a lower state which can be accessed by the DD-type operator, but whose spectral weight is relatively small due to the F-type wall source. To check this and to dig
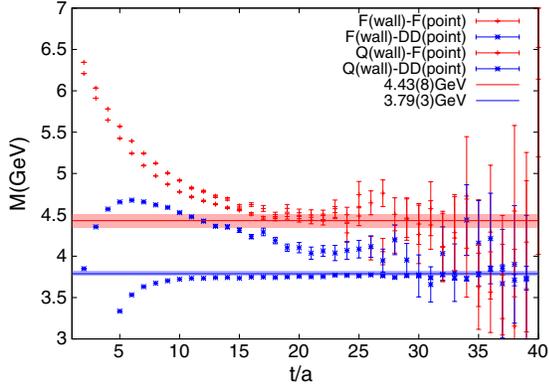
FIG. 1 (color online). The 2^{-+} effective masses of *F-F*, *DD-F*, *F-Q*, and *DD-Q* correlators at $\beta = 2.8$ are plotted for illustration. *F-F* and *F-Q* effective masses lie on each other and saturate to the same plateau with the best-fit mass $M = 4.43(8)$ GeV (indicated by the red line with the jackknife error band). The *DD-Q* effective mass has a plateau at $M = 3.79(3)$ (blue line with the jackknife error band). In contrast, the *DD-F* effective mass does not show a perfect plateau, but it evolves gradually from the upper plateau to the lower.

out the desired 2^{-+} charmonium state, we try instead another wall source operator (T_2 irreps for example),

$$|\epsilon_{ijk}|\sum_{\vec{x},\vec{y},\vec{z}} \bar{c}^a(\vec{x},0)\gamma_j c'^a(\vec{x},0)\bar{c}'^b(\vec{y},0)\Sigma_k c^b(\vec{z},0) \quad (Q\text{-type}),$$

where $\Sigma_k = \epsilon_{ijk}\sigma_{ij}$, and c' stands for a quark field with the same mass as that of the charm quark but a different flavor. For simplicity, we call this operator Q-type in the context. With this type of wall source operator, the effective masses of the F-type point sink correlator (F-Q) and DD type point sink correlator (DD-Q) are also plotted in Fig. 1, where one can find that the mass plateau of the F-Q correlator coincides with that of the F-F correlator within errors, while the effective mass of the DD-Q correlator
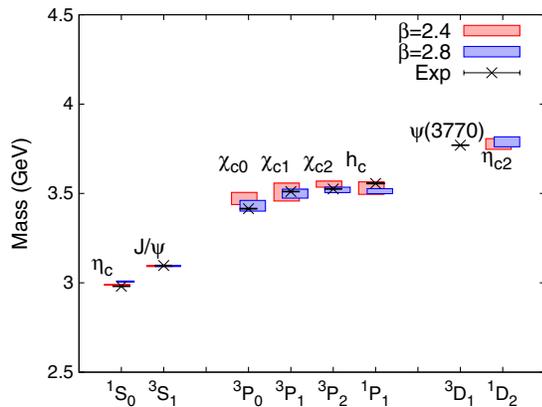

FIG. 2 (color online). $1S$, $1P$, and $1D$ charmonium spectrum. The red boxes illustrate the results for $\beta = 2.4$, and the blue ones, for $\beta = 2.8$. The experimental value are also plotted with points for comparison.

TABLE II. Listed here are the masses of the lowest-lying charmoinum states extracted from the two lattices ($\beta = 2.4$ and $\beta = 2.8$) in this work. The experimental results [5] and the nonrelativistic quark model predictions [19] are also given for comparison.

Meson	J^{PC}	$M(2.4)$	$M(2.8)$	Expt.	QM
$\eta_c(^1S_0)$	0^{-+}	2.989(2)	3.007(3)	2.981	2.982
$J/\psi(^3S_1)$	1^{--}	3.094(3)	3.094(3)	3.097	3.090
$h_c(^1P_0)$	1^{+-}	3.530(35)	3.513(14)	3.526	3.516
$\chi_{c0}(^3P_0)$	0^{++}	3.472(34)	3.431(30)	3.415	3.424
$\chi_{c1}(^3P_1)$	1^{++}	3.508(50)	3.499(25)	3.511	3.505
$\chi_{c2}(^3P_2)$	2^{++}	3.552(17)	3.520(15)	3.556	3.556
$\psi''(^3D_1)$	1^{--}	$\cdots$	$\cdots$	3.770	3.785
$\eta_{c2}(^1D_2)$	2^{-+}	3.777(30)	3.789(28)	$\cdots$	3.799

shows a very nice plateau with the best-fit mass 3.79 (3) GeV. Since the lower state has a mass close to the potential model prediction of 2^{-+} charmonium and the higher state is much heavier, we assign the lower state to the conventional $^1D_2$ charmonium state η_{c2}. This assignment can be reinforced by comparison with the established 1^3D_1 charmonium state $\psi(3770)$: They are both D-wave charmonia and are therefore close in mass; the small mass splitting can be attributed to the different spin-spin and spin-orbital interactions.

The whole spectrum of the lowest-lying charmonium states we extracted in this work is illustrated in Fig. 2 and listed in Table II, where the experimental values are also given for comparison. Since we have only two lattice spacings, we would not carry out a serious extrapolation to the continuum limit, but we show all the results, from which one can see that the effects of the finite lattice artifacts and the quenched approximation are not that important.

The goal of the spectroscopy study in this work is twofold. First, the physical spectrum of experimentally established charmonium states can be well reproduced in our formalism. This gives us confidence in our prediciton of the η_{c2} mass. Second, the practical study finds that the DD-type operator is preferable for producing the 2^{-+} charmonium. Therefore, in the study of its radiative transition, we choose the DD-type operator for η_{c2} in the calculation of the related three-point functions.

B. Renormalization of the vector current

In the quenched approximation, since there are no sea quarks, the electromagnetic current contributing to the radiative transitions of charmonia involves only the charm quark, say, $j_{em}(x) = Q_c j^\mu(x)$ with $j^\mu(x) = \bar{c}\gamma_\mu c(x)$, which is the one we adopt in this study. It is a conserved vector current and need not be renormalized in the continuum. However, on a finite lattice, it is not conserved anymore due to the lattice artifact and receives a multiplicative renormalization factor $Z_V(a_s)$. Following the scheme
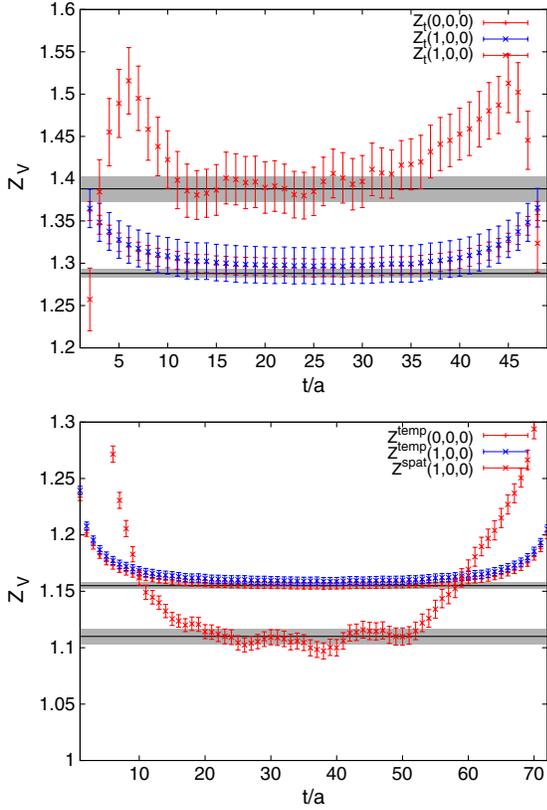
FIG. 3 (color online). The renormalization constant Z_V of the vector current. The upper panel is for $\beta = 2.4$ and the lower one for $\beta = 2.8$. The dots are the simulation data with jackknife errors, and the lines show the fit results.

proposed by Ref. [33], $Z_V(a_s)$ is extracted using the ratio of the η_c two-point function and the related three-point function evaluated at $Q^2 = 0$,

$$Z_V^{(\mu)}(t) = \frac{p^\mu}{E(\vec{p})} \frac{\frac{1}{2}\Gamma_{\eta_c}^{(2)}(\vec{p}; t_f = \frac{n_t}{2})}{\Gamma^{(3),\mu}(\vec{p}, \vec{p}, \frac{n_t}{2}, t)},$$

where the factor $1/2$ accounts for the effect of the temporal periodic boundary condition, and the superscript μ of $Z_V(a_s)$ is used to differentiate the temporal component from the spatial ones, since they are not necessarily the same due to the anisotropic lattices we use. Figure 3 plots $Z_V^{(\mu)}(t)$ with respect to t for the two lattices. Z_V's are extracted from the plateaus, and the values are listed in

TABLE III. The renormalization constants $Z_V^{(s)}$ and $Z_V^{(t)}$ of the spatial and temporal components of the vector current for $\beta = 2.4$ and $\beta = 2.8$ lattices. Two momentum modes, (0,0,0) and (1,0,0), are used for the derivation.

β	$Z_V^{(t)}(0, 0, 0)$	$Z_V^{(t)}(1, 0, 0)$	$Z_V^{(s)}(1, 0, 0)$
2.4	1.288(5)	1.299(11)	1.388(15)
2.8	1.155(3)	1.159(3)	1.110(7)

Table III. Obviously, the spatial components $Z_V^{(s)}(a)$ deviate from the temporal ones by a few percent. This deviation can be attributed to the imperfect tuning of the bare velocity in the fermion action. In this work, only $Z_V^{(s)}$'s enter the calculation, since only the spatial components of the vector current are involved in the extraction of the form factors.

C. Three-point functions and form factors

With the prescriptions discussed above, we now give a brief description of the calculation of the three-point functions. In practice, we use local sink and source operators for the initial and the final states, and insert the vector current $j^\mu(x) = \bar{c}\gamma^\mu c(x)$ only on the quark line. (The current insertion on the antiquark line is numerically equivalent and is taken into consideration by multiplying by a factor of 2 in the final result.) The three-point functions contributed by the connected diagrams (disconnected diagrams are neglected) are calculated by using the standard sequential source technique. (One can refer to Refs. [33,34] for the details.) In order to increase the statistics, we repeat the same calculations T times (where T is the temporal lattice size) by setting a point source on a different time slice each time. With the related two-point functions calculated accordingly, a straightforward way to extract the interested matrix elements $\langle f(\vec{p}', r_f)|j^\mu(0)|i(\vec{p}, r_i)\rangle$ is to fit the three-point function and two-point function simultaneously according to Eqs. (5) and (6). However, it is known that the excited states contribute much to two-point and three-point functions when the time ranges t and $t_f - t$ are not large enough. This situation is more serious for local operators, so it is not trivial to isolate the contribution of ground states. A way around this is to employ the ratios of correlation functions, which can suppress the contribution of excited states substantially. For this purpose, we introduce the functions $R^\mu(t)$,

$$R^\mu(t) = \Gamma^{(3)}(\vec{p}_f, \vec{q}, t_f, t)$$

$$\times \sqrt{\frac{2E_i\Gamma_i^{(2)}(\vec{p}_i, t_f - t)}{\Gamma_i^{(2)}(\vec{p}_i, t)\Gamma_i^{(2)}(\vec{p}_i, t_f)}} \sqrt{\frac{2E_f\Gamma_f^{(2)}(\vec{p}_f, t)}{\Gamma_f^{(2)}(\vec{p}_f, t_f - t)\Gamma_f^{(2)}(\vec{p}_f, t_f)}},$$

$$\tag{9}$$

which should be insensitive to the variation of t in a time window, so that the desired matrix element $\langle f(\vec{p}_f, r_f)|j^\mu(0)|\psi|i(\vec{p}_i, r_i)\rangle$ can be extracted from the plateau.

In the data analysis, we divide the 1000 configurations into 100 bins and use each bin average as an independent measurement. For the resultant 100 bins, we use the one-eliminating jackknife method. Since the energies $E_{i,f}$ can be determined much precisely from the two-point functions, they are treated as known parameters in the above equation. Practically, $R^\mu(t)$ is fitted by the function

$$R^\mu(t) = \langle f(\vec{p}_f, r_f)|j^\mu(0)|\psi|i(\vec{p}_i, r_i)\rangle + \delta f(t), \quad (10)$$

where the additional term $\delta f(t) = ae^{-\delta mt}$ accounts for the residual contribution of excited states. Thus we can obtain a jackknife ensemble of the matrix elements. The second step of data analysis is to extract the form factors that enter the calculation of decay widths. Since these matrix elements can be expressed in terms of form factors through the multipole decomposition,

$$\langle f(\vec{p}_f, r_f)|j^\mu(0)|i(\vec{p}_i, r_i)\rangle = \sum_k \alpha_k^\mu(p_i, p_f)\hat{F}_k(Q^2), \quad (11)$$

and $\alpha_k^\mu(p_i, p_f)$ are theoretically known kinematic functions, the form factors $\hat{F}_k(Q^2)$ can then be derived straightforwardly. Taking into consideration the contribution of the current insertion on the antiquark line, the electric charge of the charm quark $Q_c = 2/3$, and the renormalization constant of the spatial components of the current operator $Z_V^{(s)}$, $\hat{F}_k$ is related to F_k of Eq. (7) as

$$F_k(Q^2) = 2 \times \frac{2}{3}e \times Z_V^{(s)}\hat{F}_k(Q^2). \quad (12)$$

With this in mind, in the following context, we omit the hat of $\hat{F}$ and insert $Z_V^{(s)}$ implicitly in possible expressions.

In order to take good care of the correlation between the form factors, we carry out correlated minimal χ^2 fits with the jackknife covariance matrix built from the jackknife ensemble of the matrix elements. On the other hand, for a specific Q^2, there may be several symmetric copies of the matrix elements with the same value of α_k^μ. These copies are averaged over to increase statistics.

In the following subsections, we present first the calculation of the process $\chi_{c2} \to \gamma J/\psi$ to see how precisely the form factors—and thereby the transition width—can be derived, and then the results of $\eta_{c2} \to \gamma\psi$.

D. $\chi_{c2} \to \gamma J/\psi$ transition

The Minkowski space-time matrix elements for this transition can be expressed in terms of form factors as follows:

$$\langle V(\vec{p}_V, \lambda_V)|j^\mu(0)|T(\vec{p}_T, \lambda_T)\rangle = \alpha_1^\mu E_1(Q^2) + \alpha_2^\mu M_2(Q^2)$$
$$+ \alpha_3^\mu E_3(Q^2) + \alpha_4^\mu C_1(Q^2)$$
$$+ \alpha_5^\mu C_2(Q^2), \quad (13)$$

where V stands for the 1^{--} vector meson J/ψ, T stands for the 2^{++} tensor χ_{c2}, and α_i^μ are Lorentz-covariant kinematic functions of p_V and p_T (and specific polarizations of V and T), whose explicit expressions are tedious and omitted here. Although a $J = 2$ representation of the rotational symmetry in the continuum breaks into the E and T_2 irreducible representations (irreps) of the lattice spatial symmetry group O, we find that this breaking effect is small in our work, as is manifested by the near degeneracy of the masses and spectral weights of the ground states in

these two irreps when we study the relevant two-point functions. Thus, we assume that the rotation symmetry breaking is also negligible for the related matrix elements, and we carry out the multipole decomposition on the basis of $E \oplus T_2$, which is equivalent to the $J = 2$ basis up to an orthogonal transformation. One can find the detailed decomposition procedure in Appendix A and may also refer to Refs. [33,35]. In the practical study, we set T to be at rest and let V move with different spatial momenta $\vec{p} = 2\pi\vec{n}/L$. The 27 momentum modes of $\vec{n} = (n_1, n_2, n_3)$ ranging from (0,0,0) to (2,2,2) are calculated for V.

The transition width of $\chi_{c2} \to \gamma J/\psi$ for an on-shell photon ($Q^2 = 0$) involves only the form factors $E_1(0)$, $M_2(0)$, and $E_3(0)$, or explicitly,

$$\Gamma(\chi_{c2} \to \gamma J/\psi) = \frac{16\alpha|\vec{k}|}{45M_{\chi_{c2}}^2}(|E_1(0)|^2 + |M_2(0)|^2 + |E_3(0)|^2),$$
$$(14)$$

where $|\vec{q}| = (M_{\chi_{c2}}^2 - M_{J/\psi}^2)/2M_{\chi_{c2}}$ is the decaying energy of the photon and $\alpha = e^2/(4\pi)$ is the fine structure constant. Since our simulation data are obtained at $Q^2 \neq 0$, these on-shell form factors should be interpolated to $Q^2 = 0$. In doing this, we adopt the fitting functional form inspired by the nonrelativistic quark model [33],

$$F_k(Q^2) = F_k(0)(1 + \lambda_k Q^2)e^{-\frac{Q^2}{16\beta_k^2}}, \quad (15)$$

which has been applied successfully in previous works. Here $F_k(0)$, λ_k, and β_k are the parameters to be fitted though a correlated χ^2 fitting procedure where the covariance matrix is constructed using the one-eliminating jackknife method. Plotted in Fig. 4 are the extracted form factors $E_1(Q^2)$, $M_2(Q^2)$, and $E_3(Q^2)$ versus Q^2 for the two lattices of $\beta = 2.4$ (the upper panel) and $\beta = 2.8$ (the lower panel). The data points are the simulation results, and the lines are the fit function with the jackknife error bands. One can find that the data are very precise owing to the high statistics, and the fit errors are also very small. We also carry out a simple polynomial fit with respect to Q^2, $F_k(Q^2) = F_k(0) + c_1 Q^2 + c_2 Q^4$, and get consistent results within errors. Table IV lists the results of the interpolation, where the continuum limit extrapolation is also given. It is seen that the electric dipole (E_1) contribution is dominant in the transition $\chi_{c2} \to \gamma J/\psi$, while the contribution of the magnetic quadrupole (M_2) is drastically suppressed, as depicted by the ratio

$$a_2 = \frac{M_2(0)}{\sqrt{E_1(0)^2 + M_2(0)^2 + E_3(0)^2}}, \quad (16)$$

for which we get a result $a_2 = -0.107(3)$ for $\beta = 2.4$ and $a_2 = -0.082(7)$ for $\beta = 2.8$. After a linear extrapolation in a_s^2, we get the value in the continuum limit $a_2 = -0.067(7)$, which is consistent with the PDG data, where
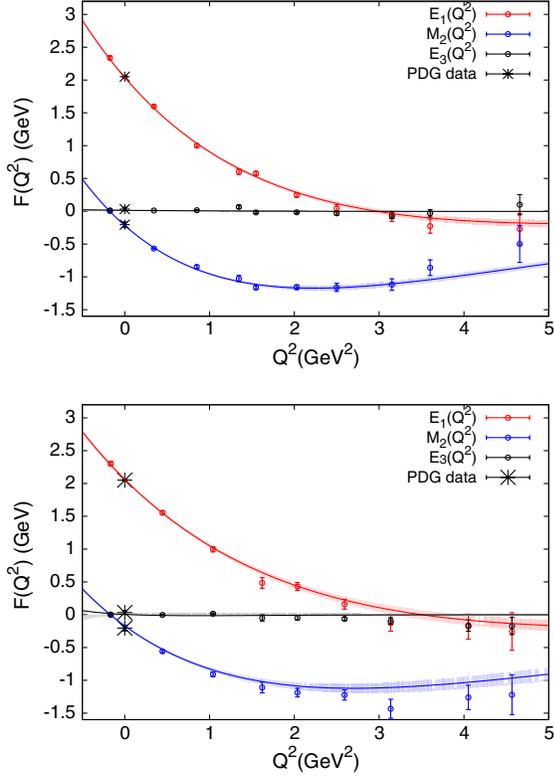
FIG. 4 (color online). The extracted form factors $E_1(Q^2)$, $M_2(Q^2)$, and $E_3(Q^2)$ are plotted versus Q^2 for the two lattices of $\beta = 2.4$ (the upper panel) and $\beta = 2.8$ (the lower panel), where the points are the simulation data, the line the fit function, and the error bands the jackknife ones. The PDG values of $E_1(0)$ and $M_2(0)$ are also plotted for comparison.

$a_2 = -0.100 \pm 0.015$ [5]. The contribution of the electric octupole E_3 is far smaller. For the ratio

$$a_3 = \frac{E_3(0)}{\sqrt{E_1(0)^2 + M_2(0)^2 + E_3(0)^2}}, \qquad (17)$$

we obtain $a_3 = 0.007(2)$ for $\beta = 2.4$, $a_3 = 0.003(4)$ for $\beta = 2.8$, and the continuum limit $a_3 = -0.003(6)$, which are also compatible with the PDG data $a_3 = 0.016 \pm 0.013$ [5]. If we focus on E_1, we get the fitting parameters β_1 and λ_1

$$\beta_1 = 0.431(5) \text{ GeV}, \qquad \lambda_1 = -0.285(2) \text{ GeV}^{-2} \quad (18)$$

TABLE IV. Listed here are the results of the interpolated form factors $E_1(0)$, $M_2(0)$, and $E_3(0)$, as well as the transition widths. The continuum limits are also given. All the results are in physical units. The widths can be compared with the PDG data $\Gamma = 380(30)$ keV [5].

β	E_1 (GeV)	M_2 (GeV)	E_3 (GeV)	Γ (keV)
2.4	2.04(2)	−0.218(4)	0.014(3)	347 ± 20
2.8	2.08(2)	−0.171(10)	0.005(8)	352 ± 11
Cont.	2.11(2)	−0.141(15)	−0.007(12)	361 ± 9

for $\beta = 2.4$ and

$$\beta_1 = 0.395(4) \text{ GeV}, \qquad \lambda_1 = -0.336(3) \text{ GeV}^{-2} \quad (19)$$

for $\beta = 2.8$.

Using the interpolated form factors $F_k(0)$ and taking the fine structure constant $\alpha = 1/137$, the transition width can be calculated directly. As shown in Table IV, the partial decay width of $\Gamma(\chi_{c2} \rightarrow J/\psi\gamma)$ is determined to be 347 ± 20 keV and 352 ± 11 keV for the two lattices, respectively. The continuum extrapolation gives $\Gamma = 361 \pm 9$ keV. All these results can be compared with the PDG average of 380(30) keV. The agreement with experimental data of the $\chi_{c2} \rightarrow J/\psi\gamma$ transition indicates that our method for the $\chi_{c2} \rightarrow J/\psi$ transition is reliable. Then we can turn to the transition $\eta_{c2} \rightarrow \gamma J/\psi$.

E. $\eta_{c2} \rightarrow J/\psi\gamma$ transition

The general Lorentz decomposition of the Minkowski matrix elements responsible for the transition $\eta_{c2} \rightarrow \gamma J/\psi$ can be expressed as

$$\langle V(\vec{p}_V, \lambda_V)|j^\mu(Q^2)|T(\vec{p}_T, \lambda_T)\rangle$$
$$= a(Q^2)A^\mu + b(Q^2)B^\mu + c(Q^2)C^\mu$$
$$+ d(Q^2)D^\mu + e(Q^2)E^\mu, \qquad (20)$$

where T stands now for the tensor meson η_{c2}; $a(Q^2)$, $b(Q^2)$, $c(Q^2)$, $d(Q^2)$, and $e(Q^2)$ are Lorentz-invariant scalar functions of Q^2; and A^μ, B^μ, C^μ, D^μ are kinematic functions whose explicit expressions can be found in Appendix B. With the multipole decomposition, the matrix elements can be also expressed in terms of the form factors M_1, E_2, M_3, and C_2:

$$\langle V(\vec{p}_V, \lambda_V)|j^\mu(0)|T(\vec{p}_T, \lambda_T)\rangle = i\alpha_1^\mu M_1(Q^2) + i\alpha_2^\mu E_2(Q^2)$$
$$+ i\alpha_3^\mu M_3(Q^2)$$
$$- i\alpha_4^\mu C_2(Q^2), \qquad (21)$$

where α_i^μ are also kinematic functions which can be expressed in terms of the kinematic functions in Eq. (20). (See Appendix B.) With real photons in the transition $\eta_{c2} \rightarrow \gamma J/\psi$, only three multipoles are contributing: the magnetic dipole (M_1), the electric quadrupole (E_2), and M_3. The transition width is written as

$$\Gamma(\eta_{c2} \rightarrow \gamma J/\psi)$$
$$= \frac{16\alpha|\vec{q}|}{45M_{\eta_{c2}}^2}(|M_1(0)|^2 + |E_2(0)|^2 + |M_3(0)|^2). \quad (22)$$

Since they are calculated at $Q^2 \neq 0$, the multipole amplitudes should be interpolated to $Q^2 = 0$. The form factor $C_2(Q^2)$ corresponds to the emission of longitudinal photons and does not contribute at $Q^2 = 0$. In extracting the amplitudes, we take the standard procedure as described in Sec. II. The three-point functions are calculated by setting the tensor at rest and making the vector moving. In analogy

with the 2^{++} case, the effect of rotational symmetry breaking between T_2 irreps and E irreps is found to be small in this case and is neglected in the data analysis. The form factors $M_1(Q^2)$, $E_2(Q^2)$, and $M_3(Q^2)$ with various Q^2 are extracted jointly by a correlated fitting with a one-eliminating jackknife covariance matrix, and the results are illustrated in Fig. 5 as data points with jackknife errors. In the following discussion, we will focus on the interpolation procedure. What is interesting is the relation between the two sets of form factors. We should first

mention that the form factors, given the fact that they are functions of Q^2, can also be written in terms of another Lorentz invariant variable, Ω:

$$\Omega \equiv (p_V \cdot p_T)^2 - m_V^2 m_T^2$$
$$= \frac{1}{4}[(m_V + m_T)^2 + Q^2][(m_V - m_T)^2 + Q^2]. \quad (23)$$

Thus, the two sets of form factors are related to each other as follows:

$$M_1(\Omega) = i\frac{\sqrt{\Omega}}{m_T}\left[\sqrt{\frac{5}{12}}(a\, m_V + a\, m_T - 2c\, m_T) + \frac{2a\, m_V - 3c\, m_T - 4d\, m_V^2 m_T + 6e\, m_V m_T^2}{4\sqrt{15}}\left(\frac{\Omega}{m_V^2 m_T^2}\right)\right.$$
$$\left. + \frac{-2a\, m_V + 3c\, m_T}{16\sqrt{15}}\left(\frac{\Omega}{m_T^2 m_V^2}\right)^2 + O\left(\left(\frac{\Omega}{m_T^2 m_V^2}\right)^3\right)\right],$$

$$E_2(\Omega) = i\frac{\sqrt{\Omega}}{m_T}\left[-\sqrt{\frac{3}{4}}(a\, m_T - a\, m_V) + \frac{2a\, m_V - c\, m_T - 4d\, m_V^2 m_T + 2e\, m_V m_T^2}{4\sqrt{3}}\left(\frac{\Omega}{m_V^2 m_T^2}\right)\right.$$
$$\left. + \frac{-2a\, m_V + c\, m_T}{16\sqrt{3}}\left(\frac{\Omega}{m_T^2 m_V^2}\right)^2 + O\left(\left(\frac{\Omega}{m_T^2 m_V^2}\right)^3\right)\right],$$

$$M_3(\Omega) = i\frac{\sqrt{\Omega}}{m_T}\left[-\frac{-a\, m_V - c\, m_T + 2d\, m_V^2 m_T + 2e\, m_V m_T^2}{\sqrt{15}}\left(\frac{\Omega}{m_V^2 m_T^2}\right) - \frac{a\, m_V + c\, m_T}{4\sqrt{15}}\left(\frac{\Omega}{m_T^2 m_V^2}\right)^2 + O\left(\left(\frac{\Omega}{m_T^2 m_V^2}\right)^3\right)\right]. \quad (24)$$

It is seen that each multipole form factor can be expressed as a series of $\Omega/(m_V^2 m_T^2)$ with a prefactor $\sqrt{\Omega}/m_T$. In the rest frame of T (as is the case in our calculation), the expression of Ω is simplified as $\Omega = (m_T|\vec{p}_V|)^2$, such that $\Omega/(m_V^2 m_T^2) = v^2$, with $v = |\vec{p}_V|/m_V$ being the spatial velocity of V. The convergence of the series in v is guaranteed if the form factors a, b, c, d, e are not singular in Q^2, since $v < 1$ (For our calculation, the largest value of v is approximately 0.5). So, for the decaying T at rest, we have the simplified expression of the form factors M_1, E_2, and M_3:

$$M_1 = |\vec{p}_V|(A_1(Q^2) + B_1(Q^2)v^2 + C_1(Q^2)v^4 + O(v^6)),$$
$$E_2 = |\vec{p}_V|(A_2(Q^2) + B_2(Q^2)v^2 + C_2(Q^2)v^4 + O(v^6)),$$
$$M_3 = |\vec{p}_V|(B_3(Q^2)v^2 + C_3(Q^2)v^4 + O(v^6)). \quad (25)$$

With these expressions, the following information can be inferred: (i) The desired $|\vec{p}_V|$ prefactor accounting for the P-wave decay of $\eta_{c2} \to \gamma J/\psi$ is explicitly derived. (ii) The leading contribution to M_1 and E_2 is of order $O(1)$, while that of M_3 is of order $O(v^2)$. For the case of this study, since $v_{\max} \sim 0.5$, it is reasonable that the nonsingular A_i, B_i and C_i can be expanded with respect to v, such that we can take the following functions to do the interpolation:

$$F_i(v) = Av + Bv^3 + Cv^5 + O(v^6)(F_i \to M_1, E_2),$$
$$F_i(v) = Bv^3 + Cv^5 + Dv^7 + O(v^9)(F_i \to M_3), \quad (26)$$

and the on-shell amplitudes $M_1(Q^2 = 0)$, $E_2(Q^2 = 0)$, and $M_3(Q^2 = 0)$ can be reached by $F_i(v_0)$ with $v_0 = (m_T^2 - m_V^2)/(2m_T m_V)$. The extracted form factor and the interpolation are shown in Fig. 5, where the data points are the simulated results with jackknife errors. One can see that at $v = 0$ [corresponding to $Q^2 = -(m_T - m_V)^2 \sim 0.5$ GeV^2] the form factors M_1, E_2, and M_3 are surely consistent with zero. The fits using Eq. (26) are also shown as curves with jackknife error bands. The interpolated values of these form factors at $Q^2 = 0$ for both $\beta = 2.4$ and $\beta = 2.8$ are listed in Table V, where the resultant transition widths and the corresponding continuum limits are also given. It is surprising that, for both lattices, the obtained $|M_3|$ is unexpectedly large and comparable to M_1. This may be qualitatively attributed to recoiling effects of the charm quark or charm antiquark by emitting the hard photon with an energy $E_\gamma \sim 0.6$ GeV in this transition, which may result in large form factors $d(Q^2)$ and $e(Q^2)$ (see the discussion below). In contrast to the mild dependence of M_1 and M_3 on the lattice spacing, the form factor E_2 is very sensitive to the lattice spacing. The reason for this is unclear and under investigation. Anyway, after a naive continuum extrapolation using the data from the two lattices in this work, we get the continuum results of the form factors as follows:

$$M_1 = 0.104(10) \text{ GeV}, \qquad E_2 = -0.071(20) \text{ GeV},$$
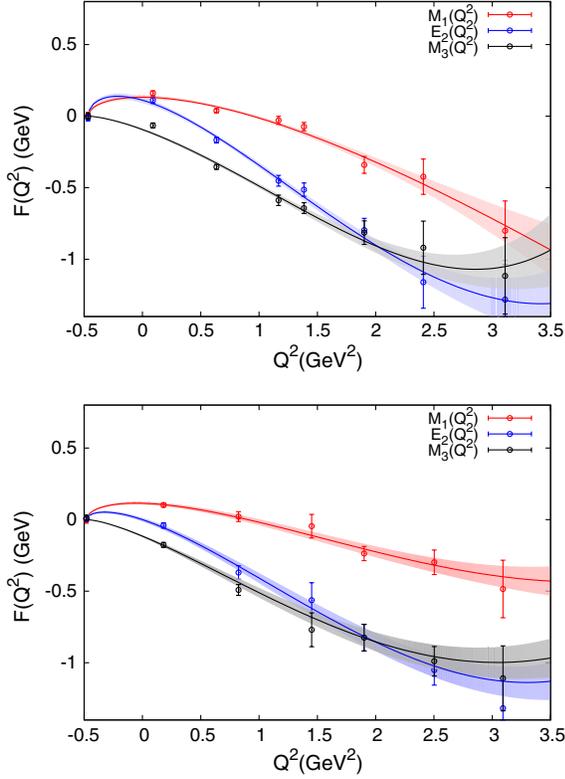$$M_3 = -0.132(10) \text{ GeV}. \quad (27)$$

FIG. 5 (color online). The $\eta_{c2} - J/\psi$ transition form factors $M_1(Q^2)$, $E_2(Q^2)$, and $M_3(Q^2)$ are plotted versus Q^2 for the two lattices of $\beta = 2.4$ (the upper panel) and $\beta = 2.8$ (the lower panel), respectively. The points are the simulation data, and the lines illustrate the fit function with jackknife error bands.

Applying these results to Eq. (22), the transition width of $\eta_{c2} \to \gamma J/\psi$ is predicted to be

$$\Gamma(\eta_{c2} \to \gamma J/\psi) = 3.8 \pm 0.9 \text{ keV}. \quad (28)$$

There have also been several phenomenological studies on this transition, one of which is in the framework of the light-front quark model [27], where the on-shell transition amplitude is decomposited as

$$\langle V(\vec{p}_V, \lambda_V)|j^\mu(0)|\eta_2(\vec{p}_T, \lambda_T)\rangle$$
$$= [2f_1 \epsilon^{\mu\nu\rho\sigma} p_\nu^T p_\rho^V \epsilon_\sigma^\beta(\vec{p}_T, \lambda_T) \epsilon_\beta^*(\vec{p}_V, \lambda_V)$$
$$+ (f_2 + f_3) \epsilon^{\mu\nu\rho\sigma} p_\nu^T p_\rho^V \epsilon_\sigma^*(\vec{p}_V, \lambda_V) \epsilon^{\alpha\beta}(\vec{p}_T, \lambda_T) p_\alpha^V p_\beta^V$$
$$+ 2f_4 \epsilon^{\mu\nu\rho\sigma} p_\nu^T p_\rho^V \epsilon_\sigma^\beta(\vec{p}_T, \lambda_T) p_\beta^V \epsilon^{*\alpha}(\vec{p}_V, \lambda_V) p_\alpha^T], \quad (29)$$

and the effective couplings are determined to be

$$f_1 = -0.0140(2) \text{ GeV}^{-1}, \quad f_2 = 0.146(3) \text{ GeV}^{-3},$$
$$f_3 = -0.092(1) \text{ GeV}^{-3}, \quad f_4 = 0.0180(1) \text{ GeV}^{-3}. \quad (30)$$

Since this decomposition is equivalent to Eq. (20) by the relation

$$c(0) = 2f_1, \quad d(0) = -(f_2 + f_3), \quad e(0) = -2f_4 \quad (31)$$

TABLE V. Listed here are the interpolated values of the form factors M_1, E_2, and M_3 at $Q^2 = 0$ for both $\beta = 2.4$ and $\beta = 2.8$. The resultant transition widths and the corresponding continuum limits are also given.

β	M_1 (GeV)	E_2 (GeV)	M_3 (GeV)	Γ (keV)
2.4	0.133(13)	0.111(17)	−0.093(9)	4.4 ± 0.9
2.8	0.115(11)	−0.0007(14)	−0.117(9)	3.1 ± 0.6
Cont.	0.104(10)	−0.071(20)	−0.132(10)	3.8 ± 0.9

[It should be noted that $a(Q^2)$ and $b(Q^2)$ are equal to zero when $Q^2 = 0$ because they are proportional to $C_2(Q^2)$.], the corresponding multipole amplitudes can be calculated from Eq. (24) as

$$M_1 = 0.079(2) \text{ GeV}, \qquad E_2 = -0.086(2) \text{ GeV},$$
$$M_3 = -0.125(3) \text{ GeV}, \quad (32)$$

which gives a width of $\Gamma = 3.54(12)$ keV. Taking into consideration the uncertainty of the choice of parameters such as the charm quark mass m_c and the wave function parameter, etc., one can find that the lattice results and the LFQM results are surprisingly in excellent agreement. On the other hand, with the values in Eq. (30), we find that the coefficients $B_i(Q^2)$ of the v^2 term in Eq. (25) are surely much larger than $A_i(Q^2)$ at $Q^2 = 0$ so as to compensate for the suppression of v^2. This explains to some extent the fact that the M_3 in this transition competes with M_1 and E_2.

The other phenomenological study [28] applying the nonrelativistic QCD (NRQCD) gives the transition width as

$$\Gamma(\eta_{c2} \to \gamma J/\psi) = \frac{8\alpha|\vec{k}|^3}{675m_c^2}(a_1^2 + a_2^2 + a_3^2), \quad (33)$$

where a_1, a_2, and a_3 are equivalent to the standard form factors M_1, E_2, and M_3 up to a constant factor and are calculated explicitly in NRQCD. By comparing this equation with Eq. (14), the factor is approximately 0.33 GeV, say, $F_i \simeq (0.33 \text{ GeV})a_i$. Thus, their work gives the predictions

$$M_1 \sim 0.026\text{–}0.045 \text{ GeV}, \quad E_2 \simeq M_3 \simeq -0.13 \text{ GeV}, \quad (34)$$

which are also in reasonable agreement with our results.

IV. CONCLUSION

We calculate in the quenched approximation the mass of $J^{PC} = 2^{-+}$ charmonium η_{c2}, as well as its radiative transition width to J/ψ. The computations are carried out on two anisotropic lattices with different lattice spacings, such that the lattice artifacts can be controlled to some extent. As a calibration, we calculate first the spectrum of the lowest-lying charmonia, such as $1S$ and $1P$ states, and reproduce the physical pattern of the spectrum. In addition, we calculate the transition width of $\chi_{c2} \to \gamma J/\psi$ and get

the result 361 ± 9 keV, which is in good agreement with the experimental value of 380 ± 30 keV. Both of these facts manifest the small systematic uncertainties due to the quenched approximation and the finite lattice spacings.

There are two states observed in the 2^{-+} channel, with masses of 3.80(3) GeV and 4.43(8) GeV. The lower state has a mass similar to that of the well-established $\psi(3770)$, which is always assigned to be mainly the 1^3D_1 charmonium, and therefore can be naturally identified as the conventional 1^1D_2 charmonium η_{c2}. Obviously, it is about 70 MeV lower in mass than $X(3872)$, and this difference cannot be attributed to the systematic uncertainties of our work.

As for the transition rate of $\eta_{c2} \to J/\psi\gamma$, we get a small partial width of roughly 3.8(9) keV, which is in agreement with the phenomenological studies. Taking the branch ratio $\mathrm{Br}(X(3872) \to J/\psi\gamma) > 0.9\%$ (*BABAR*) or 0.6% (Belle), the full width of $X(3872)$ is estimated to be <420–630 keV, which is smaller than, but not in contradiction with the experimental upper limit $\Gamma_X < 1.2$ MeV. Obviously, a reliable calculation of the partial width $\eta_{c2} \to \psi'\gamma$ is also crucial for the $^1D_2$ charmonium assignment of $X(3872)$, but unfortunately there are difficulties in the unambiguous extraction of excited states on the lattice. However, we can still infer some useful information from the calculation of $\eta_{c2} \to J/\psi\gamma$. In the potential quark model, it is known that $^1D_2 \to \gamma V$ is a hindered transition with $M_1(0) = 0$; therefore, the observed nonzero $M_1(0)$ and the appearance of the higher multipoles E_2 and M_3

can be understood as the relativistic correction and the recoil effects of the emission of a hard photon ($E_\gamma \sim 0.65$ GeV for the final J/ψ and $E_\gamma \sim 0.11$ GeV for ψ'). Intuitively, this kind of effect for the final ψ' can be similar to that for the final J/ψ, or even milder; thus, the width of $\eta_{c2} \to \gamma\psi'$ will be suppressed by a kinematic factor of $(0.65/0.11)^3 \sim 200$ when compared with the transition $\eta_{c2} \to \gamma J/\psi$. With this fact in mind, the η_{c2} assignment of $X(3872)$ can be ruled out if *BABAR*'s observation of $\mathrm{Br}(X(3872) \to \gamma\psi')/\mathrm{Br}(X(3872) \to \gamma J/\psi) = 3.4 \pm 1.4$ is confirmed.

APPENDIX A: MULTIPOLE DECOMPOSITION OF $\chi_{c2} \leftrightarrow J/\psi$

For the convenience of readers, the details of the multipole decomposition of matrix elements of the electromagnetic current $j^\mu(0)$ between a 1^{--} vector V state and a 2^{++} tensor state are described here following Ref. [35]. The most general Lorentz-covariant decomposition with P and C parity invariance is

$$\langle V(\vec{p}_V, \lambda_V)|j^\mu(0)|T(\vec{p}_T, \lambda_T)\rangle = a(Q^2)A^\mu + b(Q^2)B^\mu + c(Q^2)C^\mu + d_T(Q^2)D_T^\mu + d_V(Q^2)D_V^\mu + f_T(Q^2)F_T^\mu + f_V(Q^2)F_V^\mu, \quad (A1)$$

with the definitions

$$A^\mu \equiv \epsilon^{\mu\nu}(\vec{p}_T, \lambda_T)\epsilon_\nu^*(\vec{p}_V, \lambda_V), \qquad B^\mu \equiv \epsilon^{\mu\nu}(\vec{p}_T, \lambda_T)p_\nu^V(\epsilon^*(\vec{p}_V, \lambda_V)\cdot p_T), \qquad C^\mu \equiv \epsilon^{*\mu}(\vec{p}_V, \lambda_V)(\epsilon^{\alpha\beta}(\vec{p}_T, \lambda_T)p_\alpha^V p_\beta^V),$$

$$D_T^\mu \equiv p_T^\mu(\epsilon^{\alpha\beta}(\vec{p}_T, \lambda_T)\epsilon_\alpha^*(\vec{p}_V, \lambda_V)p_\beta^V), \qquad D_V^\mu \equiv p_V^\mu(\epsilon^{\alpha\beta}(\vec{p}_T, \lambda_T)\epsilon_\alpha^*(\vec{p}_V, \lambda_V)p_\beta^V),$$

$$F_T^\mu \equiv p_T^\mu(\epsilon^{\alpha\beta}(\vec{p}_T, \lambda_T)p_\alpha^V p_\beta^V)(\epsilon^*(\vec{p}_V, \lambda_V)\cdot p_T), \qquad F_V^\mu \equiv p_V^\mu(\epsilon^{\alpha\beta}(\vec{p}_T, \lambda_T)p_\alpha^V p_\beta^V)(\epsilon^*(\vec{p}_V, \lambda_V)\cdot p_T). \quad (A2)$$

On the other hand, the matrix elements $\langle V|j^\mu|T\rangle$ can be also expressed in terms of the helicity amplitudes:

$$\langle V|j^\mu|T\rangle\epsilon_\mu^*(\lambda_\gamma = \pm) = \sum_k \sqrt{\frac{2k+1}{2J+1}}[E_k\frac{1}{2}(1 + (-1)^k\delta P) \mp M_k\frac{1}{2}(1 - (-1)^k\delta P)]\langle k\mp; J'\lambda \pm 1|J\lambda\rangle, \quad (A3)$$

$$\langle V|j^\mu|T\rangle\epsilon_\mu^*(\lambda_\gamma = 0) = \sum_k \sqrt{\frac{2k+1}{2J+1}}C_k\frac{1}{2}(1 + (-1)^k\delta P)\langle k0; J'\lambda|J\lambda\rangle, \quad (A4)$$

where E_k, M_k, and C_K are multipole amplitudes, and δP is the product of the P parity of the initial (T) and final (V) states, taking the value $\delta P = -1$ for the $2^+ \to 1^-$ transition. These are actually the helicity selection rules. An additional constraint comes from the conservation of the vector current,

$$\langle V|j^\mu|T\rangle q_\mu = \partial_\mu\langle V|j^\mu|T\rangle = 0. \quad (A5)$$

With the constraints of Eqs. (A3)–(A5), we can solve $a(Q^2)$, $b(Q^2)$, $c(Q^2)$, ... in the rest frame of the initial state with the spatial momentum of the photon parallel to the z axis. [The polarization vector of the photon takes $(1,0,0,1)$.] Thus, we can get the expressions in terms of $E_k(q^2)$, $C_K(Q^2)$. After that, the general expression of the form factor $a, b, c, \ldots$ can be

obtained by carrying out a general Lorentz transformation. For the case of the $2^+ \to 1^-$ transition here, Eq. (A3) provides three independent equations with respect to the three different helicities of the vector state, and therefore gives the relations between $[a(Q^2), b(Q^2), c(Q^2)]$ and $[E_1(Q^2), M_2(Q^2), E_3(Q^2)]$ as

$$a = \frac{E_3}{\sqrt{15}} - M_2\sqrt{3} + \sqrt{\frac{3}{5}}E_1,$$

$$b = \frac{1}{5\sqrt{3}\Omega}(3\sqrt{5}E_1(m_T m_V - p_T.p_V) + 5M_2(m_I m_V + p_T.p_V) - \sqrt{5}E_3(4m_T m_V + p_T.p_V)), \qquad \text{(A6)}$$

$$c = m_T^2 \frac{\sqrt{5}E_3 + 4M_2}{2\sqrt{3}\Omega},$$

with $\Omega \equiv (p_T \cdot p_V)^2 - m_T^2 m_V^2$. The constraints from Eqs. (A4) and (A5) with the plus/minus helicity of the vector meson can fix the parameters d_V and d_T. Furthermore, f_V and f_T can be derived from Eqs. (A4) and (A5) with zero helicity of the vector meson. As such, the multipole decomposition of the matrix elements $\langle V|j^\mu|T\rangle$ can be expressed finally as

$$\langle V(\vec{p}_V, \lambda_V)|j^\mu(Q^2)|T(\vec{p}_T, \lambda_T)\rangle = \alpha_1^\mu E_1(Q^2) + \alpha_2^\mu M_2(Q^2) + \alpha_3^\mu E_3(Q^2) + \alpha_4^\mu C_1(Q^2) + \alpha_5^\mu C_3(Q^2), \qquad \text{(A7)}$$

with the functions α_i^μ defined by

$$\alpha_1^\mu = \sqrt{\frac{3}{5}}\left[-A^\mu + \frac{m_T}{\Omega}(\tilde{\omega} - m_V)B^\mu + \frac{m_T}{\Omega}(\tilde{\omega}D_T^\mu - m_T D_V^\mu) + \frac{m_T^2}{\Omega^2}(\tilde{\omega} - m_V)(-\tilde{\omega}F_T^\mu + m_T F_V^\mu) \right],$$

$$\alpha_2^\mu = \sqrt{\frac{1}{3}}\left[A^\mu - \frac{m_T}{\Omega}(\tilde{\omega} + m_V)B^\mu - \frac{2m_T^2}{\Omega}C^\mu + \frac{m_T}{\Omega}(-\tilde{\omega}D_T^\mu + m_T D_V^\mu) + \frac{m_T^2}{\Omega^2}((\tilde{\omega}^2 + \tilde{\omega}m_V - 2m_V^2)F_T^\mu + m_i(\tilde{\omega} - m_V)F_V^\mu) \right],$$

$$\alpha_3^\mu = \sqrt{\frac{1}{15}}\left[-A^\mu + \frac{m_T}{\Omega}(\tilde{\omega} + 4m_V)B^\mu - \frac{5m_T^2}{2\Omega}C^\mu + \frac{m_T}{\Omega}(\tilde{\omega}D_T^\mu - m_T D_V^\mu) \right.$$
$$\left. + \frac{m_T^2}{\Omega^2}\left(-\left(\tilde{\omega}^2 + 4\tilde{\omega}m_V + \frac{5}{2}m_V^2\right)F_T^\mu + m_i\left(\frac{7}{2}\tilde{\omega} + 4m_V\right)F_V^\mu \right) \right],$$

$$\alpha_4^\mu = \sqrt{\frac{3}{5}}\frac{m_T}{\Omega\sqrt{q^2}}\left[(m_V^2 - \tilde{\omega}m_T)D_T^\mu + (m_T^2 - \tilde{\omega}m_T)D_V^\mu - \frac{m_T}{\Omega}(\tilde{\omega} - m_V)((m_V^2 - \tilde{\omega}m_T)F_T^\mu + (m_T^2 - \tilde{\omega}m_T)F_V^\mu) \right],$$

$$\alpha_5^\mu = \sqrt{\frac{2}{5}}\frac{m_T}{\Omega\sqrt{q^2}}\left[(m_V^2 - \tilde{\omega}m_T)D_T^\mu + (m_T^2 - \tilde{\omega}m_T)D_V^\mu - \frac{m_T}{\Omega}\left(\tilde{\omega} + \frac{3}{2}m_V\right)((m_V^2 - \tilde{\omega}m_T)F_T^\mu + (m_T^2 - \tilde{\omega}m_T)F_V^\mu) \right], \qquad \text{(A8)}$$

where $\tilde{\omega} \equiv \frac{p_T.p_V}{m_T}$ and $\omega^\pm \equiv p_T.p_V \pm m_V m_T$.

APPENDIX B: MULTIPOLES OF $\eta_{c2} \leftrightarrow J/\psi$

The case of $\eta_{c2} \to J/\psi$ is sightly different from that above. The most general Lorentz-covariant decomposition with P and C parity invariance is

$$\langle V(\vec{p}_V, \lambda_V)|j^\mu(0)|\eta_2(\vec{p}_T, \lambda_T)\rangle = a(Q^2)A^\mu + b(Q^2)B^\mu + c(Q^2)C^\mu + d(Q^2)D^\mu + e(Q^2)E^\mu, \qquad \text{(B1)}$$

with

$$A^\mu = \epsilon^{\mu\nu\rho\sigma}\epsilon_\nu^*(\vec{p}_V, \lambda_V)p_\rho^V \epsilon_\sigma^\beta(\vec{p}_T, \lambda_T)p_\beta^V, \qquad B^\mu = \epsilon^{\beta\nu\rho\sigma}p_\beta^T \epsilon_\nu^*(\vec{p}_V, \lambda_V)p_\rho^V \epsilon_\sigma^\mu(\vec{p}_T, \lambda_T),$$

$$C^\mu = \epsilon^{\mu\nu\rho\sigma}p_\nu^T p_\rho^V \epsilon_\sigma^\beta(\vec{p}_T, \lambda_T)\epsilon_\beta^*(\vec{p}_V, \lambda_V), \qquad D^\mu = \epsilon^{\mu\nu\rho\sigma}p_\nu^V p_\rho^T \epsilon_\sigma^*(\vec{p}_V, \lambda_V)\epsilon^{\alpha\beta}(\vec{p}_T, \lambda_T)p_\alpha^V p_\beta^V,$$

$$E^\mu = \epsilon^{\mu\nu\rho\sigma}p_\nu^V p_\rho^T \epsilon_\sigma^\beta(\vec{p}_T, \lambda_T)p_\beta^V \epsilon^{*\alpha}(\vec{p}_V, \lambda_V)p_\alpha^T. \qquad \text{(B2)}$$

In fact, there exist another three Lorentz-covariant structures A_T, E_V, and E_T:

$$E_V^\mu = \epsilon^{\alpha\nu\rho\sigma} p_\alpha^T \epsilon_\beta^*(\vec{p}_V, \lambda_V) p_\rho^V \epsilon^{\sigma\beta}(\vec{p}_T, \lambda_T) p_\beta^V p_V^\mu, \qquad A_T^\mu = \epsilon^{\mu\nu\rho\sigma} \epsilon_\nu^*(\vec{p}_V, \lambda_V) p_\rho^T \epsilon_\sigma^\beta(\vec{p}_T, \lambda_T) p_\beta^V,$$

$$E_T^\mu = \epsilon^{\alpha\nu\rho\sigma} p_\alpha^T \epsilon_\beta^*(\vec{p}_V, \lambda_V) p_\rho^V \epsilon^{\sigma\beta}(\vec{p}_T, \lambda_T) p_\beta^V p_T^\mu, \tag{B3}$$

which, however, are not independent and can be expressed in terms of the functions in Eq. (B2):

$$A_T^\mu = -B^\mu - C^\mu, \qquad E_T^\mu = m_T^2 A^\mu + p_V \cdot p_T B^\mu + p_V \cdot p_T C^\mu + E^\mu, \qquad E_V^\mu = p_V \cdot p_T A^\mu + m_V^2 B^\mu + m_V^2 C^\mu + D^\mu. \tag{B4}$$

So they do not appear in the decomposition. Based on this, one can follow the similar procedure of the case of $\chi_{c2} \to J/\psi$ to derive the related multipole decomposition. The constraints of decomposition are similar to Eqs. (A3) and (A5) while $\delta P = 1$. Finally, one can get the result

$$\begin{aligned}
\langle V(\vec{p}_V, \lambda_V)|j^\mu(0)|\eta_2(\vec{p}_T, \lambda_T)\rangle &= \frac{iM_1(Q^2)}{5\Omega^{1/2}}\left[-\sqrt{15}C^\mu + \frac{1}{\Omega}\sqrt{15}E^\mu(-m_V m_T + p_T \cdot p_V)\right] \\
&\quad + \frac{iE_2(Q^2)}{3\Omega^{1/2}}\left[\sqrt{3}C^\mu + \frac{1}{\Omega}(2\sqrt{3}D^\mu m_T^2 - \sqrt{3}E^\mu(m_V m_T + p_T \cdot p_V))\right] \\
&\quad + \frac{iM_3(Q^2)}{30\Omega^{1/2}}\left[-2\sqrt{15}C^\mu + \frac{1}{\Omega}(5\sqrt{15}D^\mu m_T^2 + 2\sqrt{15}E^\mu(4m_V m_T + p_T \cdot p_V))\right] \\
&\quad - \frac{iC_2(Q^2)}{\sqrt{q^2}\Omega^{1/2}}\left[A^\mu m_T + B^\mu m_T + C^\mu m_T + \frac{1}{\Omega}(D^\mu m_T(m_T^2 - p_T \cdot p_V)\right. \\
&\quad \left. + E^\mu m_T(m_V^2 - p_T \cdot p_V))\right]. \tag{B5}
\end{aligned}$$

APPENDIX C: FORM FACTORS AS A FUNCTION OF Q^2 OR Ω

Transition form factors are always expressed as Lorentz scalar functions of the squared momentum transfer, $Q^2 = -q^2 = -(q_i - q_f)^2$, where p_i and p_f refer to the four-momenta of the initial and final particles, respectively. However, if one looks into the Lorentz decomposition [Eq. (A1)] and the multipole decomposition [Eq. (A7)] for the $\chi_{c2} \to J/\psi$ transition matrix elements, one can find that the quantity $\Omega \equiv (p_i \cdot p_f)^2 - m_i^2 m_f^2$, with $p_i \cdot p_f = (m_i^2 + m_f^2 + Q^2)/2$, is also an interesting Lorentz-invariant kinematic variable. According to Eq. (A6), the multipole amplitudes E_1, M_2, and E_3 can be reversely expressed in terms of the form factors a, b, c as

$$E_1(\Omega) = \sqrt{\frac{5}{3}}a + \frac{6c\,m_V - 3a\,m_T + 4b\,m_V^2 m_T}{4\sqrt{15}m_T}\left(\frac{\Omega}{m_V^2 m_T^2}\right) - \frac{1}{16}\sqrt{\frac{3}{5}}a\left(\frac{\Omega}{m_V^2 m_T^2}\right)^2 + O\left(\left(\frac{\Omega}{m_V^2 m_T^2}\right)^3\right),$$

$$M_2(\Omega) = \frac{2c\,m_V - a\,m_T + 4b\,m_V^2 m_T}{4\sqrt{3}m_T}\left(\frac{\Omega}{m_V^2 m_T^2}\right) - \frac{a}{16\sqrt{3}}\left(\frac{\Omega}{m_V^2 m_T^2}\right)^2 + O\left(\left(\frac{\Omega}{m_V^2 m_T^2}\right)^3\right), \tag{C1}$$

$$E_3(\Omega) = \frac{-2c\,m_V + (a + 2b\,m_V^2)m_T}{\sqrt{15}m_T}\left(\frac{\Omega}{m_V^2 m_T^2}\right) + \frac{a}{4\sqrt{15}}\left(\frac{\Omega}{m_V^2 m_T^2}\right)^2 + O\left(\left(\frac{\Omega}{m_V^2 m_T^2}\right)^3\right).$$

Obviously, these are polynomials of the variable $\Omega/(m_V^2 m_T^2)$ with the coefficients the combinations of the form factors a, b, c. The physical meaning of the above expression can be understood in the rest frame of the decaying particle (T here), where $\Omega/(m_V^2 m_T^2) = v^2$ with $v = |\vec{p}_V|/m_V \sim 0.16$ for the $\chi_{c2} \to J/\psi$ transition. It is clearly seen from these expressions that the E_1 transition is dominant, while M_2 and E_3 transitions are suppressed by a factor of $v^2 \sim 0.026$. On the other hand, $M_2(Q^2)$ and $E_3(Q^2)$ should be zero at $v = 0$, or equivalently, $Q^2 = -(m_T - m_V)^2$, as is confirmed by our simulation results (seen in Fig. 4). It is found in the calculation that M_2 and E_3 are consistent with zero when both the initial and final states are at rest.

As for the $\eta_{c2} \to J/\psi$ transition, the multipole amplitudes M_1, E_2, and M_3 can similarly be expressed as polynomials in $\Omega/(m_V^2 m_T^2)$, where the coefficients are also the combinations of the form factors in Eq. (B1):

$$M_1(\Omega) = i\frac{\sqrt{\Omega}}{m_T}\left[\sqrt{\frac{5}{12}}(a\,m_V + a\,m_T - 2c\,m_T) + \frac{2a\,m_V - 3c\,m_T - 4d\,m_V^2 m_T + 6e\,m_V m_T^2}{4\sqrt{15}}\left(\frac{\Omega}{m_V^2 m_T^2}\right)\right.$$

$$\left. + \frac{-2a\,m_V + 3c\,m_T}{16\sqrt{15}}\left(\frac{\Omega}{m_T^2 m_V^2}\right)^2 + O\left(\left(\frac{\Omega}{m_T^2 m_V^2}\right)^3\right)\right],$$

$$E_2(\Omega) = i\frac{\sqrt{\Omega}}{m_T}\left[-\sqrt{\frac{3}{4}}(a\,m_T - a\,m_V) + \frac{2a\,m_V - c\,m_T - 4d\,m_V^2 m_T + 2e\,m_V m_T^2}{4\sqrt{3}}\left(\frac{\Omega}{m_V^2 m_T^2}\right)\right.$$

$$\left. + \frac{-2a\,m_V + c\,m_T}{16\sqrt{3}}\left(\frac{\Omega}{m_T^2 m_V^2}\right)^2 + O\left(\left(\frac{\Omega}{m_T^2 m_V^2}\right)^3\right)\right],$$

$$M_3(\Omega) = i\frac{\sqrt{\Omega}}{m_T}\left[-\frac{-a\,m_V - c\,m_T + 2d\,m_V^2 m_T + 2e\,m_V m_T^2}{\sqrt{15}}\left(\frac{\Omega}{m_V^2 m_T^2}\right) - \frac{a\,m_V + c\,m_T}{4\sqrt{15}}\left(\frac{\Omega}{m_T^2 m_V^2}\right)^2 + O\left(\left(\frac{\Omega}{m_T^2 m_V^2}\right)^3\right)\right]. \quad \text{(C2)}$$

In the rest frame of the decaying particle η_{c2} (denoted by T here), the prefactor $\sqrt{\Omega}/m_T = |\vec{p}_V|$ is exactly the requirement of the P-wave decay of $\eta_{c2} \to \gamma J/\psi$. The physical implication of these expressions has been discussed in context and is omitted here.

---

[1] S. K. Choi *et al.* (Belle Collaboration), Phys. Rev. Lett. **91,** 262001 (2003).

[2] B. Aubert *et al.* (*BABAR* Collaboration), Phys. Rev. D **71,** 071103 (2005).

[3] D. E. Acosta *et al.* (CDF II Collaboration), Phys. Rev. Lett. **93,** 072001 (2004).

[4] V. M. Abazov *et al.* (D0 Collaboration), Phys. Rev. Lett. **93,** 162002 (2004).

[5] J. Beringer *et al.* (Particle Data Group), Phys. Rev. D **86,** 010001 (2012).

[6] S.-K. Choi, S. L. Olsen, K. Trabelsi *et al.* (Belle Collaboration), Phys. Rev. D **84,** 052004 (2011).

[7] A. Abulencia *et al.* (CDF Collaboration), Phys. Rev. Lett. **96,** 102002 (2006).

[8] B. Aubert *et al.* (*BABAR* Collaboration), Phys. Rev. D **74,** 071101 (2006).

[9] C. Bignamini, B. Grinstein, F. Piccinini, A. D. Polosa, and C. Sabelli, Phys. Rev. Lett. **103,** 162001 (2009).

[10] M. B. Voloshin, Phys. Lett. B **579,** 316 (2004).

[11] I. W. Lee, A. Faessler, T. Gutsche, and V. E. Lyubovitskij, Phys. Rev. D **80,** 094005 (2009).

[12] L. Maiani, F. Piccinini, A. D. Polosa, and V. Riquer, Phys. Rev. D **71,** 014028 (2005).

[13] S. Dubnicka, A. Z. Dubnickova, M. A. Ivanov, and J. G. Korner, Phys. Rev. D **81,** 114007 (2010).

[14] S. Dubnicka, A. Z. Dubnickova, M. A. Ivanov, J. G. Korner, P. Santorelli, and G. G. Saidullaeva, Phys. Rev. D **84,** 014006 (2011).

[15] P. del Amo Sanchez *et al.* (*BABAR* Collaboration), Phys. Rev. D **82,** 011101 (2010).

[16] J. S. Lange *et al.* (Belle Collaboration), arXiv:1109.1699.

[17] B. Aubert *et al.* (*BABAR* Collaboration), Phys. Rev. Lett. **102,** 132001 (2009).

[18] V. Bhardwaj *et al.* (Belle Collaboration), Phys. Rev. Lett. **107,** 091803 (2011).

[19] T. Barnes, S. Godfrey, and E. S. Swanson, Phys. Rev. D **72,** 054026 (2005).

[20] M. Okamoto *et al.*, Phys. Rev. D **65,** 094508 (2002).

[21] P. Chen, Phys. Rev. D **64,** 034509 (2001).

[22] Y. Chen, C. Liu, Y. B. Liu, J. P. Ma, and J. B. Zhang, arXiv:hep-lat/0701021.

[23] L. M. Liu, S. M. Ryan, M. Peardon, G. Moir, and P. Vilaseca, Proc. Sci. LATTICE2011 (2011) 140; L. M. Liu, G. Moir, M. Peardon, S. M. Ryan, C. E. Thomas, P. Vilaseca, J. J. Dudek, R. G. Edwards, B. Joó, and D. G. Richards (Hadron Spectrum Collaboration), J. High Energy Phys. 07 (2012) 126.

[24] T. Barnes and S. Godfrey, Phys. Rev. D **69,** 054008 (2004).

[25] A. M. Badalian, V. L. Morgunov, and B. L. G. Bakker, Phys. At. Nucl. **63,** 1635 (2000).

[26] Y. S. Kalashnikova and A. V. Nefediev, Phys. Rev. D **82,** 097502 (2010).

[27] H. W. Ke and X. Q. Li, Phys. Rev. D **84,** 114026 (2011).

[28] Y. Jia, W. L. Sang, and J. Xu, arXiv:1007.4541.

[29] C. J. Morningstar and M. Peardon, Phys. Rev. D **56,** 4043 (1997).

[30] C. Liu, J. Zhang, Y. Chen, and J. P. Ma, Nucl. Phys. **B624,** 360 (2002).

[31] S. Su, L. Liu, X. Li, and C. Liu, Int. J. Mod. Phys. A **21,** 1015 (2006); Chin. Phys. Lett. **22,** 2198 (2005).

[32] X. Liao and T. Manke, arXiv:hep-lat/0210030.

[33] J. J. Dudek, R. G. Edwards, and D. G. Richards, Phys. Rev. D **73,** 074507 (2006).

[34] F. D. R. Bonnet, R. G. Edwards, G. T. Fleming, R. Lewis, and D. G. Richards, Phys. Rev. D **72,** 054506 (2005).

[35] J. J. Dudek, R. G. Edwards, and C. E. Thomas, Phys. Rev. D **79,** 094504 (2009).